

# Unified State Feedback Control of a Hybrid Distribution Transformer using Particle Swarm Optimization Tuning

Dave Figueroa\*  
dave.figueroa.dokt@pw.edu.pl

Alvaro Carreno\*  
alvaro.carreno@pw.edu.pl

Mariusz Malinowski\*  
malin@isep.pw.edu.pl

Liu Yang†  
yangliu\_424@sina.com

Zhihong Zhao†‡  
zhihongzhao@stu.hit.edu.cn

\* Institute of Control and Industrial Electronics, Warsaw University of Technology, Warsaw, Poland.

† Research Institute of Interdisciplinary Intelligent Science, Ningbo University of Technology, Ningbo, China.

‡ Research Institute of Intelligent Control and Systems, Harbin Institute of Technology, Harbin, China.

**Abstract**—This paper presents a unified state feedback control strategy for a hybrid distribution transformer (HDT) using particle swarm optimization (PSO) for tuning the control gains. The proposed control strategy aims to achieve zero steady-state error for sinusoidal references and disturbances while ensuring good dynamic performance. An augmented state-space model of the HDT is developed, incorporating the delays introduced by the digital control system and resonant states to eliminate steady-state errors. The control gains are optimized using PSO to minimize a cost function that considers both transient and steady-state performance. Simulation results demonstrate the effectiveness of the proposed control strategy in regulating the voltage and current of the HDT under various operating conditions.

**Index Terms**—hybrid distribution transformer, optimal control, state-feedback control, particle swarm optimization

## I. INTRODUCTION

THE increasing penetration of renewable energy sources in the electrical grid has led to a significant rise in the use of power electronic converters. These converters are essential for integrating RES into the grid, as they facilitate the conversion of DC power generated by sources like solar panels and wind turbines into AC power compatible with the grid [1]. However, the widespread use of power electronic converters has also introduced challenges related to power quality, such as the injection of harmonics and non-linear loads, which can lead to voltage distortions and other issues in the electrical grid [2], [3].

There are many solutions that have been proposed to address the power quality issues in the grid, such as static compensators (STATCOMs) [4], dynamic voltage restorers (DVRs) [5], active power filters (APFs) [6], unified power quality conditioners (UPQC) [7] and the solid-state transformers (SST) [8]. SSTs has the ability to mitigate most of the power quality issues mentioned above, while also providing galvanic isolation and voltage transformation. However, the high cost and complexity of SSTs has limited their widespread adoption in the distribution grid and, also, does not provide the same short-circuit current capability as traditional distribution transformers (DTs) [9].

For this reason, the hybrid distribution transformer (HDT) emerges as a promising solution to address the disadvantages of SSTs while still providing advanced power quality functionalities. The HDT is a power electronic transformer that combines the functions of a traditional distribution transformer with those of power electronic converters [10], [11]. Many HDT configurations have been proposed in the literature, and in consequence, classifications have been made [9]. One of the classifications is based on the source of the converter's energy, i.e., whether the energy is obtained from a capacitor/battery, the primary or secondary side of the DT, or an auxiliary winding. On the other hand, the other classification is based on how the converters inject energy into the system, i.e., whether they are connected in series or in parallel with the DT.

Several control strategies have been proposed for the HDT in the literature, including finite control set model predictive control (FCS-MPC) [12], decoupled control strategies, such as the resonant control [11] the compound controller [13], quasi-proportional controller [14] and the separated state-feedback controller [15]. While these approaches have demonstrated good performance, they often rely on heuristic parameter tuning or treat the resonant compensation separately from the state feedback framework, which complicates the design and limits systematic optimization.

In this paper, a unified control strategy based on state feedback control with resonant states is proposed for the HDT. This control strategy aims to achieve zero steady-state error for sinusoidal references and disturbances, while also ensuring good dynamic performance. The control strategy also considers the inherent delay present in real control microcontrollers. Moreover, instead of adjusting the feedback weights heuristically, as in conventional LQR designs, the proposed approach leverages particle swarm optimization (PSO) to automatically tune the control gains according to a cost function that balances transient and steady-state performance. This approach had been previously used for tuning the control gains for a VSI, achieving good results [16], [17]. The proposed control strategy is validated through simulation results that demonstrate its effectiveness in regulating the voltage and

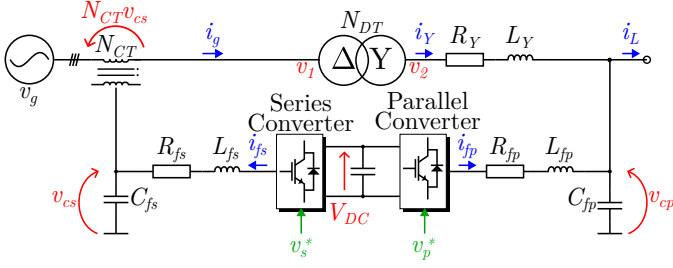


Fig. 1. Hybrid distribution transformer circuit diagram.

current of the HDT under various operating conditions.

## II. MODEL OF THE HYBRID DISTRIBUTION TRANSFORMER

The HDT configuration used in this paper is shown in Fig. 1. It consists of a traditional DT connected to two back-to-back VSCs: a series converter connected to the primary of the DT through a CT, and a parallel converter connected in parallel to the load, which is connected to the secondary of the DT. All the state-space equations are derived in the  $\alpha\beta$  reference frame, until otherwise specified.

### A. Series Converter

The objectives of the series converter are to compensate for voltage disturbances, e.g. sags, swells and harmonics that may occur in the grid. This is done by injecting a voltage in series with the grid through the CT. The dynamics of the series converter are given by the following state-space equation:

$$\dot{x}_s = \underbrace{\begin{bmatrix} -\frac{R_{fs}}{L_{fs}} \mathbf{I} & -\frac{1}{L_{fs}} \mathbf{I} \\ \frac{1}{C_{fs}} \mathbf{I} & \mathbf{0} \end{bmatrix}}_{\mathbf{A}_s} x_s + \underbrace{\begin{bmatrix} \frac{1}{L_{fs}} \\ 0 \end{bmatrix}}_{\mathbf{B}_s} v_s + \underbrace{\begin{bmatrix} 0 \\ \frac{1}{C_{fs}} \end{bmatrix}}_{\mathbf{P}_{is}} i_s \quad (1)$$

where  $x_s = [i_{fs} \ v_{cs}]^T$  is the state vector and  $i_s$  is the currents that circulates to the CT. The parameters  $R_{fs}$ ,  $L_{fs}$ , and  $C_{fs}$  are the series converter filter resistance, inductance, and capacitance respectively.

The current  $i_s$  is related to the transformer secondary side current  $i_Y$  through  $i_s = N_{CT} i_Y$  relationship, where  $N_{CT}$  is the CT turns ratio and  $i_g$  is the grid current. The grid current can be expressed in terms of the transformer secondary side current and the parallel converter capacitor current as:

$$i_g^{abc} = \frac{1}{N_{DT}} \begin{bmatrix} 1 & 0 & -1 \\ -1 & 1 & 0 \\ 0 & -1 & 1 \end{bmatrix} i_Y^{abc} \quad (2)$$

where  $N_{DT}$  is the transformer turns ratio. Converting this to  $\alpha\beta$  coordinates gives:

$$i_g = \frac{1}{N_{DT}} \mathbf{K}_{T\alpha\beta} i_Y \quad (3)$$

where the matrix that models the  $\Delta - Y$  transformer is given by:

$$\mathbf{K}_{T\alpha\beta} = \begin{bmatrix} \frac{2}{3} & \frac{\sqrt{3}}{2} \\ -\frac{\sqrt{3}}{2} & \frac{2}{3} \end{bmatrix} \quad (4)$$

Substituting this into (1) gives:

$$\dot{x}_s = \mathbf{A}_s x_s + \mathbf{B}_s v_s + \mathbf{P}_{is} N_{CT} \frac{1}{N_{DT}} \mathbf{K}_{T\alpha\beta} i_Y \quad (5)$$

### B. Parallel Converter

In the other hand, the parallel converter is responsible for maintaining the dc-link voltage of the HDT and compensating load side disturbances, including harmonics and unbalances that can be present. The dynamics of the parallel converter are given by the following state-space equation:

$$\dot{x}_p = \underbrace{\begin{bmatrix} -\frac{R_{fp}}{L_{fp}} \mathbf{I} & -\frac{1}{L_{fp}} \mathbf{I} \\ \frac{1}{C_{fp}} \mathbf{I} & \mathbf{0} \end{bmatrix}}_{\mathbf{A}_p} x_p + \underbrace{\begin{bmatrix} \frac{1}{L_{fp}} \\ 0 \end{bmatrix}}_{\mathbf{B}_p} v_p + \underbrace{\begin{bmatrix} 0 \\ -\frac{1}{C_{fp}} \end{bmatrix}}_{\mathbf{P}_{iY}} i_Y + \underbrace{\begin{bmatrix} 0 \\ -\frac{1}{C_{fp}} \end{bmatrix}}_{\mathbf{P}_{iL}} i_L \quad (6)$$

where  $x_p = [i_{fp} \ v_{cp}]^T$  and  $i_L$  is the load current. The parameters  $R_{fp}$ ,  $L_{fp}$ , and  $C_{fp}$  are the parallel converter filter resistance, inductance, and capacitance respectively.

The secondary side voltage of the transformer  $v_2$  can be expressed in terms of the primary side voltage  $v_1$ , which is the sum of  $v_g$  and  $N_{CT} v_{cs}$ , as:

$$v_2 = \frac{1}{N_{DT}} \mathbf{K}_{T\alpha\beta}' (N_{CT} v_{cs} + v_g) \quad (7)$$

where  $\mathbf{K}_{T\alpha\beta}'$  is the transpose of  $\mathbf{K}_{T\alpha\beta}$ . Hence, the dynamics of the transformer are modeled as a series impedance referred to the  $Y$  side and its state-space equation is given by:

$$\frac{di_Y}{dt} = -\frac{R_Y}{L_Y} i_Y - \frac{1}{L_Y} v_{cp} + \frac{1}{L_Y} \frac{1}{N_{DT}} \mathbf{K}_{T\alpha\beta}' (v_g + N_{CT} v_{cs}) \quad (8)$$

where  $R_Y$  and  $L_Y$  are the transformer series resistance and leakage inductance respectively. The matrices  $\mathbf{P}_{vg} = \frac{1}{L_Y} \frac{1}{N_{DT}} \mathbf{K}_{T\alpha\beta}'$  and  $\mathbf{P}_{vc} = \frac{1}{L_Y} \frac{N_{CT}}{N_{DT}} \mathbf{K}_{T\alpha\beta}'$  are the grid voltage and series converter capacitor voltage disturbance input matrices respectively.

### C. Overall HDT Model

The overall HDT model is obtained by combining the series converter, parallel converter, and transformer state-space equations given in (1), (6), and (8) respectively. The combined state-space equations are given by:

$$\begin{aligned}
\frac{d}{dt} \begin{bmatrix} x_s \\ x_p \end{bmatrix} &= \underbrace{\begin{bmatrix} \mathbf{A}_s & \mathbf{P}_{iY}\mathbf{M}_p \\ \mathbf{P}_{vc}\mathbf{M}_s & \mathbf{A}_p \end{bmatrix}}_{\mathbf{A}} \underbrace{\begin{bmatrix} x_s \\ x_p \end{bmatrix}}_x + \underbrace{\begin{bmatrix} \mathbf{B}_s & \mathbf{0} \\ \mathbf{0} & \mathbf{B}_p \end{bmatrix}}_{\mathbf{B}} \underbrace{\begin{bmatrix} v_s \\ v_p \end{bmatrix}}_u \\
&+ \underbrace{\begin{bmatrix} \mathbf{0} \\ \mathbf{P}_{vg} \end{bmatrix}}_{\mathbf{P}_{vg}} v_g + \underbrace{\begin{bmatrix} \mathbf{0} \\ \mathbf{P}_{iL} \end{bmatrix}}_{\mathbf{P}_{iL}} i_L \\
\frac{dx(t)}{dt} &= \mathbf{A}x(t) + \mathbf{B}u(t) + \mathbf{P}_{vg}v_g(t) + \mathbf{P}_{iL}i_L(t) \\
y(t) &= \mathbf{C}x(t)
\end{aligned} \tag{9}$$

where the matrices  $\mathbf{M}_p = \begin{bmatrix} \mathbf{0} & \mathbf{I} & \mathbf{0} \end{bmatrix}$  and  $\mathbf{M}_s = \begin{bmatrix} \mathbf{0} & \mathbf{I} \end{bmatrix}$  are used to select the appropriate states from the parallel and series converter state vectors respectively.

The HDT system is discretized using a zero-order hold with a sampling time of  $T_s = 5 \mu s$ . The discrete-time state-space model is given by:

$$\begin{aligned}
x_{k+1} &= \mathbf{A}_d x_k + \mathbf{B}_d u_k + \mathbf{P}_{vg,d} v_{gk} + \mathbf{P}_{iL,d} i_{Lk} \\
y_k &= \mathbf{C} x_k
\end{aligned} \tag{10}$$

where  $\mathbf{A}_d = e^{\mathbf{A}T_s}$ ,  $\mathbf{B}_d = \int_0^{T_s} e^{\mathbf{A}\tau} d\tau \mathbf{B}$ ,  $\mathbf{P}_{vg,d} = \int_0^{T_s} e^{\mathbf{A}\tau} d\tau \mathbf{P}_{vg}$ ,  $\mathbf{P}_{iL,d} = \int_0^{T_s} e^{\mathbf{A}\tau} d\tau \mathbf{P}_{iL}$ , and  $\mathbf{C} = \mathbb{I}$ .

In most of the applications, there is a delay of one sampling period between the calculation of the control input and its application to the system. To account for this delay, the discrete-time state-space model is augmented with a new state representing the previous control input:

$$m_k = u_{k+1} \tag{11}$$

This can be expressed in state-space form as:

$$\begin{bmatrix} x_{k+1} \\ u_{k+1} \end{bmatrix} = \underbrace{\begin{bmatrix} \mathbf{A}_d & \mathbf{B}_d \\ \mathbf{0} & \mathbf{0} \end{bmatrix}}_{\mathbf{A}_{d,delay}} \begin{bmatrix} x_k \\ u_k \end{bmatrix} + \underbrace{\begin{bmatrix} \mathbf{0} \\ \mathbf{I} \end{bmatrix}}_{\mathbf{B}_{d,delay}} m_k \tag{12}$$

where  $\mathbf{A}_{d,delay}$  and  $\mathbf{B}_{d,delay}$  are the augmented system and input matrices respectively.

### III. CONTROL STRATEGY

With the state-space model of the HDT defined, the next step is to design a control strategy that ensures the desired performance.

#### A. Proposed Control Strategy

The proposed control strategy is based on a state feedback controller which is designed using the augmented state-space model of the HDT, defined in (12). The control strategy aims to achieve zero steady-state error for sinusoidal references. The state feedback controller is designed using the discrete LQR approach given by:

$$\mathbf{K} = \text{dlqr}(\mathbf{A}_{d,delay}, \mathbf{B}_{d,delay}, \mathbf{Q}, \mathbf{R}) \tag{13}$$

where  $\mathbf{Q} \in \mathbb{R}^{11}$  and  $\mathbf{R} \in \mathbb{R}^4 = \mathbf{I}$  are the state and input weighting matrices, respectively. The gain matrix is partitioned into three sub-matrices:  $\mathbf{K}_x$ ,  $\mathbf{K}_u$  and  $\mathbf{K}_r$  for convenience. The block diagram of the proposed control strategy is shown in

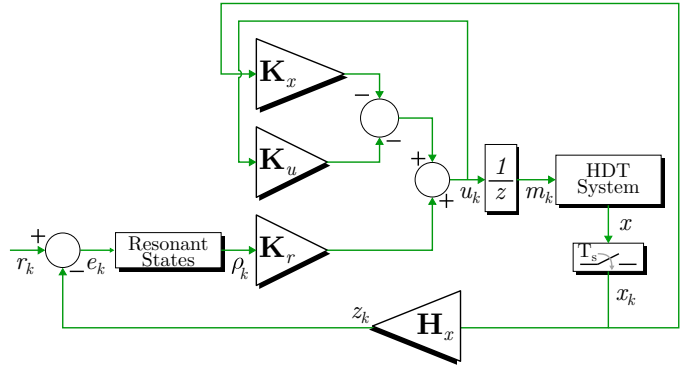


Fig. 2. Block diagram of the proposed control strategy for the HDT.

Fig. 2. With the partitioned gain matrices defined, the control input can be expressed as:

$$u_k = -\mathbf{K}_x x_k - \mathbf{K}_u u_k - \mathbf{K}_r \rho_k \tag{14}$$

where  $\mathbf{K}_x$  is the state feedback gain matrix,  $\mathbf{K}_u$  is the previous control input gain matrix and  $\mathbf{K}_r$  is the resonant states gain matrix.

The resonant states are defined by the following state-space equation:

$$\frac{d\rho(t)}{dt} = \underbrace{\begin{bmatrix} 0 & \omega \\ -\omega & 0 \end{bmatrix}}_{\mathbf{A}_r} \rho(t) + \underbrace{\begin{bmatrix} 1 \\ 0 \end{bmatrix}}_{\mathbf{B}_r} e(t) \tag{15}$$

where  $\omega$  is the nominal angular frequency and  $e(t)$  is the error vector between the reference and the measured output. Each of the references signals has two resonant states associated with it, meaning that for the HDT control, there are eight resonant states in total (4 for the  $ev_{cs,\alpha\beta}$  and 4 for the  $if_{p,\alpha\beta}$ ). This can be expressed as:

$$\frac{d\rho(t)}{dt} = \text{diag}(\mathbf{A}_r, \mathbf{A}_r, \mathbf{A}_r, \mathbf{A}_r) \rho(t) \tag{16}$$

$$+ \text{diag}(\mathbf{B}_r, \mathbf{B}_r, \mathbf{B}_r, \mathbf{B}_r) e(t) \tag{17}$$

These resonant states are then discretized using a ZOH giving the matrices  $\mathbf{A}_{rd}$  and  $\mathbf{B}_{rd}$ . The augmented state-space model of the resonant states can be expressed as:

$$\begin{bmatrix} x_{k+1} \\ u_{k+1} \\ \rho_{k+1} \end{bmatrix} = \begin{bmatrix} \mathbf{A}_{d,delay} & \mathbf{0} \\ \mathbf{B}_{rd}\mathbf{H}_x & \mathbf{A}_{rd} \end{bmatrix} \begin{bmatrix} x_k \\ u_k \\ \rho_k \end{bmatrix} + \begin{bmatrix} \mathbf{B}_{d,delay} \\ \mathbf{0} \end{bmatrix} \begin{bmatrix} m_k \\ e_k \end{bmatrix} \tag{18}$$

$$y_k = [\mathbf{C} \quad \mathbf{0}] \begin{bmatrix} x_k \\ u_k \\ \rho_k \end{bmatrix}$$

where  $\mathbf{H}_x$  selects the states from the HDT state vector that are imposed to follow references.

The series converter reference is calculated as the difference between the nominal value of the grid voltage and the actual value and the parallel converter reference is the sum of the DC-link control loop, which uses the instantaneous power theory [18], and the harmonic elimination control loop. This is based in the work from Carreno et al. [15].

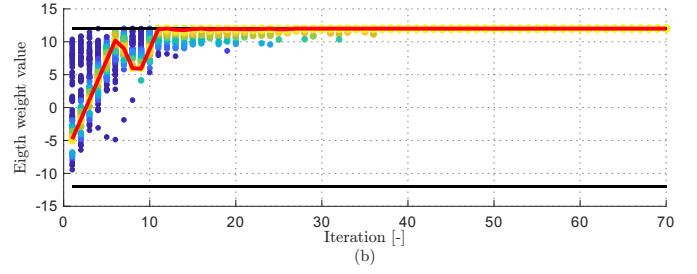
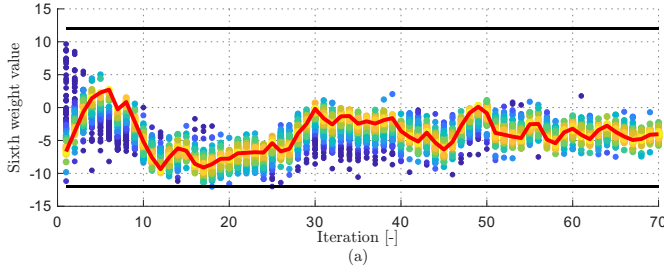


Fig. 3. Convergence of exponents over the PSO iterations. (a) Exponent  $q_6$  associated with the parallel converter inductor current  $v_{cp,\alpha\beta}$ . (b) Exponent  $q_8$  associated with the first resonant state of the error  $e1v_{cs,\alpha\beta}$ .

### B. Particle Swarm Optimization

To facilitate the tuning of the state feedback gain matrix  $\mathbf{K}$  by adjusting  $\mathbf{Q}$ , the PSO algorithm is employed to optimize the weights associated with each state in the cost function. The PSO algorithm is a population-based optimization technique inspired by the social behavior of birds and fish [19]. It consists of a swarm of particles, where each particle represents a potential solution to the optimization problem, in this case, the vector of powers  $q_{x,j}(i)$ , where  $x$ ,  $j$  and  $i$  are the state, particle and iteration numbers. The particles move through the search space, updating their positions based on their own experience and the experience of their neighbors. The velocity and position of each particle are updated using the following equations:

$$\begin{aligned} v_j(i+1) &= K_{ap}(v_j(i) + c_1 r_1(pbest_j - x_j(i)) \\ &\quad + c_2 r_2(gbest - x_j(i))) \\ x_j(i+1) &= x_j(i) + v_j(i+1) \end{aligned} \quad (19)$$

where  $v_j(i)$ ,  $x_j(i)$ ,  $pbest_j$  and  $gbest$  are the velocity, position, the best position and global-best position of the particle  $j$  at iteration  $i$ .  $c_1$  and  $c_2$  are cognitive and social acceleration coefficients,  $r_1$  and  $r_2$  are random numbers uniformly distributed in the range  $[0, 1]$ , and  $K_{ap}$  is the constriction factor given by:

$$K_{ap} = \frac{2}{2 - \phi - \sqrt{\phi^2 - 4\phi}} \quad (20)$$

where  $\phi = c_1 + c_2 > 4$  is a constant that ensures convergence.

The PSO algorithm iteratively updates the positions and velocities of the particles until the maximum of iteration number is reached. The best position found by the swarm is considered the optimal solution to the optimization problem.

### C. PSO Performance Index

The performance index used for the PSO optimization is a cost function that considers both the transient and steady-state performance of the HDT [16]. This index is minimized through many iterations considering the HDT system with step references and without any applied disturbances. The cost function is defined as:

$$J = \frac{1}{N} \sum_{i=1}^N |e_k|^2 + \beta \Delta u_k^2 \quad (21)$$

where  $N$  is the number of samples in the simulation,  $\Delta u_k$  is the change in control input at sample  $k$ , and  $\beta$  is a weighting

TABLE I  
PSO PARAMETERS USED FOR THE OPTIMIZATION OF THE CONTROL GAINS.

Parameter	Value
Number of particles	100
Maximum number of iterations	70
Maximum weight exponent for states	$[-20, 20]$
Absorbing walls boundaries	$[-12, 12]$
Cognitive acceleration coefficients ( $c_1, c_2$ )	2.05
Performance index weighting factor ( $\beta$ )	$2 \times 10^{-7}$

factor that balances the importance of the transient and steady-state performance.

The assumptions that are made when running the PSO algorithm is that the penalties for the  $\alpha$  and  $\beta$  components are equal, including the resonant terms for each of the components. For that reason, the search of space is shrunk from the 22 states to the half. Also, to simplify the search space of the swarm, the particles are applied as powers of the state weights. This can be expressed as:

$$\mathbf{Q} = \text{diag} \{10^{q_1} \mathbf{I}, 10^{q_2} \mathbf{I}, \dots, 10^{q_{11}} \mathbf{I}\} \quad (22)$$

The optimization variables lie within a define range including the absorbing walls boundaries [20] which allows obtaining a not-large LQR gain. The PSO parameters used for the optimization are listed in Table I.

TABLE II  
OPTIMIZED STATE WEIGHT EXPONENTS  $q_i$  FROM PSO.

$q_1$	$q_2$	$q_3$	$q_4$	$q_5$	$q_6$
-6.186	-7.810	-4.406	-1.642	-8.674	-5.315
$q_7$	$q_8$	$q_9$	$q_{10}$	$q_{11}$	
-11.118	11.999	9.672	10.516	8.827	

After running the PSO algorithm, each of the state weights exponents ( $q_x$ ) are given the Table II. The convergence of two of the exponents over the PSO iterations is shown in Fig. 3, while the convergence of the fitness value over the PSO iterations is shown in Fig. 4.

## IV. SIMULATION RESULTS

In this section, the simulation results of the proposed control strategy are presented. The simulations are performed using MATLAB/Simulink, and the system parameters are listed in Table III. The proposed control strategy is tested under grid unbalanced swell, load impact, load unbalance, and non-linear load conditions.

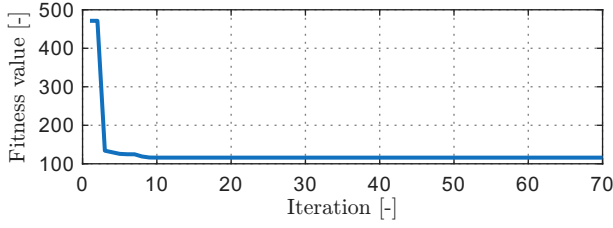


Fig. 4. Convergence of the fitness value over the PSO iterations.

TABLE III  
SYSTEM PARAMETERS

Parameter	Variable	Value
Grid Voltage	$V_g$	10 kV
Nominal Converter Voltage	$V_s$	400 V
DC Link Voltage	$V_{DC}$	700 V
Grid Frequency	$f_e$	50 Hz
Series Converter Filter Inductance	$L_{fs}$	200 $\mu$ H
Series Converter Filter Resistance	$R_{fs}$	100 m $\Omega$
Series Converter Filter Capacitance	$C_{fs}$	12 $\mu$ F
Parallel Converter Filter Inductance	$L_{fp}$	200 $\mu$ H
Parallel Converter Filter Resistance	$R_{fp}$	100 m $\Omega$
Parallel Converter Filter Capacitance	$C_{fp}$	12 $\mu$ F
Transformer Dispersion Inductance	$L_Y$	100 $\mu$ H
Transformer Series Resistance	$R_Y$	5 m $\Omega$
Coupling Transformer Turns Ratio	$N_{CT}$	5
Distribution Transformer Turns Ratio	$N_{DT}$	$V_s/(V_g\sqrt{3})$
Converters Switching Frequency	$f_{sw}$	20 kHz
Control Sampling Time	$T_s$	50 $\mu$ s

Each of the load impacts are comprised by 47  $\Omega$  resistive load per phase, 2 k $\Omega$  resistive load in phase *a* for the unbalanced load, and a three-phase diode bridge rectifier with a 47  $\Omega$  resistive load at its output for the non-linear load. The simulation results are shown in Fig. 5.

#### A. Grid Voltage Unbalanced Swell Compensation

From the instant  $t = 10$  ms until  $t = 260$  ms, a three-phase unbalanced swell of 10% the nominal value, in phase *b* is applied to the grid voltage, as shown in Fig. 5.(a). The proposed control strategy effectively compensates for the unbalanced swell, meaning that the parallel inverter injects the necessary voltage to maintain a balanced transformer secondary side current, as shown in Fig. 5.(d).

#### B. Load Impact

At  $t = 60$  ms, a three-phase balanced load impact of 47  $\Omega$  per phase is applied, as shown in Fig. 5.(b). In this case, the parallel converter injects the necessary current to maintain the transformer secondary side current, in particular after the load impact, as shown in Fig. 5.(e).

#### C. Unbalanced Load Compensation

Following the load impacts, at  $t = 100$  ms an unbalanced load is applied, where phase *a* has a load of 2 k $\Omega$  and phases *b* and *c* have a load of 47  $\Omega$ , as shown in Fig. 5.(f). The parallel converter injects the necessary current to maintain a balanced transformer secondary side current, as shown in Fig. 5.(e).

#### D. Non-linear Load Compensation

At  $t = 140$  ms, a three-phase diode bridge rectifier with a 47  $\Omega$  resistive load at its output is applied, as shown in Fig. 5.(f). In this case, the parallel converter reference is mainly composed by the fundamental component of the load current, which is extracted using a notch filter. The proposed control strategy manages to compensate this disturbance, maintaining the transformer secondary side current sinusoidal and balanced, as shown in Fig. 5.(d).

#### E. Third Harmonic Compensation

Finally, at  $t = 200$  ms, a third harmonic component is added to the grid voltage, as shown in Fig. 5.(a). In this case, the series converter reference is mainly composed by the fundamental and third harmonic components of the grid voltage, which are extracted using a notch filter. The proposed control strategy effectively compensates for this disturbance, maintaining the transformer secondary side current sinusoidal and balanced, as shown in Fig. 5.(d).

### V. CONCLUSIONS

In the present paper a unified state feedback control strategy for a HDT was proposed. The control strategy was designed using an augmented state-space model of the HDT that includes the delays introduced by the digital control system and resonant states to achieve zero steady-state error for sinusoidal references. The control gains were optimized using PSO to minimize a cost function that considers both the transient and steady-state performance of the HDT. This enables to have optimal weights choices at the hour of tuning the state feedback controller instead of relying on heuristic or try-and-error tuning.

The proposed control strategy was validated through simulation results that demonstrated its effectiveness in regulating the voltage and current of the HDT under various operating conditions, including grid voltage unbalanced swell compensation, load impact and unbalanced load compensation, non-linear load compensation, and grid harmonics compensation.

### REFERENCES

- [1] F. Blaabjerg, Y. Yang, K. A. Kim, and J. Rodriguez, "Power electronics technology for large-scale renewable energy generation," *Proceedings of the IEEE*, vol. 111, no. 4, pp. 335–355, 2023.
- [2] M. Najafzadeh, R. Ahmadihangar, O. Husev, I. Roasto, T. Jalakas, and A. Blinov, "Recent contributions, future prospects and limitations of interlinking converter control in hybrid ac/dc microgrids," *IEEE Access*, vol. 9, pp. 7960–7984, 2021.
- [3] S. Sepasi, C. Talichet, and A. S. Pramanik, "Power quality in microgrids: A critical review of fundamentals, standards, and case studies," *IEEE Access*, vol. 11, pp. 108 493–108 531, 2023.
- [4] T. Engelbrecht, A. Isaacs, S. Kynev, J. Matevosyan, B. Niemann, A. J. Owens, B. Singh, and A. Grondona, "Statcom technology evolution for tomorrow's grid: E-statcom, statcom with supercapacitor-based active power capability," *IEEE Power and Energy Magazine*, vol. 21, no. 2, pp. 30–39, 2023.
- [5] T. Kandil and M. Adel Ahmed, "Control and operation of dynamic voltage restorer with online regulated dc-link capacitor in microgrid system," *Canadian Journal of Electrical and Computer Engineering*, vol. 43, no. 4, pp. 331–341, 2020.
- [6] A. K. Mishra, S. R. Das, P. K. Ray, R. K. Mallick, A. Mohanty, and D. K. Mishra, "Pso-gwo optimized fractional order pid based hybrid shunt active power filter for power quality improvements," *IEEE Access*, vol. 8, pp. 74 497–74 512, 2020.
- [7] H. Fujita and H. Akagi, "The unified power quality conditioner: the integration of series- and shunt-active filters," *IEEE Transactions on Power Electronics*, vol. 13, no. 2, pp. 315–322, 1998.



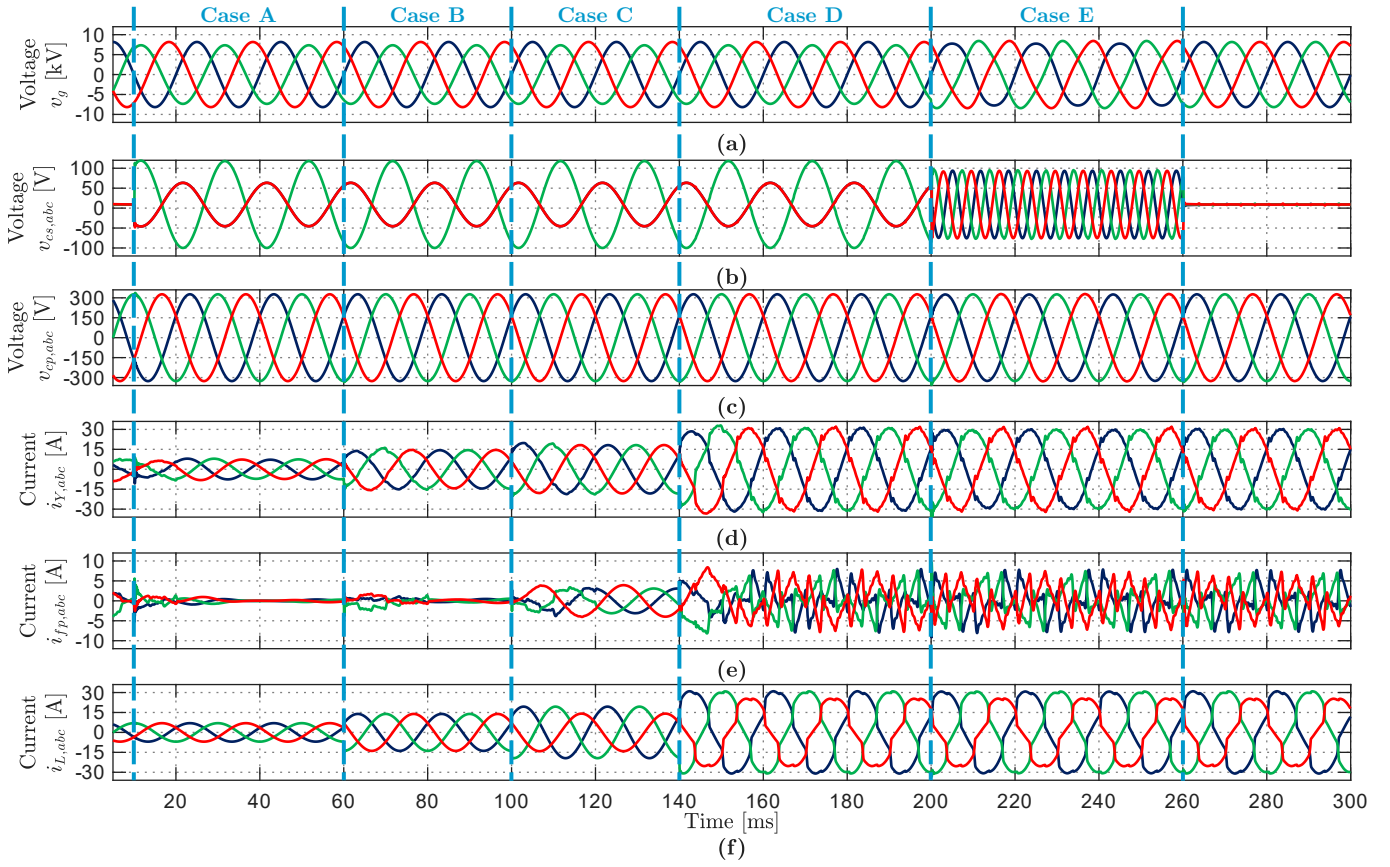


Fig. 5. Simulation results in  $abc$  coordinates for the proposed control strategy under grid and load disturbances. (a) Grid voltage, (b) Series converter output voltage, (c) Parallel converter output voltage, (d) Secondary side transformer current, (e) Parallel converter current, (f) Load current

- [8] J. E. Huber and J. W. Kolar, "Applicability of solid-state transformers in today's and future distribution grids," *IEEE Transactions on Smart Grid*, vol. 10, no. 1, pp. 317–326, 2019.
- [9] A. Carreno, M. Perez, C. Baier, A. Huang, S. Rajendran, and M. Malinowski, "Configurations, Power Topologies and Applications of Hybrid Distribution Transformers," *Energies*, vol. 14, no. 5, p. 1215, Feb. 2021.
- [10] M. Y. Haj-Maharsi, L. Tang, R. Gutierrez, and S. Bala, "Hybrid distribution transformer with ac & dc power capabilities," US Patent US20 100 201 338A1, Aug., 2010.
- [11] W. Matelski, "Badania eksperymentalne transformatora hybrydowego jako kondycjonera napięcia w sieciach typu TN," *PRZEGŁAD ELEKTROTECHNICZNY*, vol. 1, no. 5, pp. 233–238, May 2023.
- [12] P. Costa, G. Paraíso, S. F. Pinto, and J. F. Silva, "A four-leg matrix converter based hybrid distribution transformer for smart and resilient grids," *Electric Power Systems Research*, vol. 203, p. 107650, Feb. 2022.
- [13] Y. Liu, D. Liang, P. Kou, M. Zhang, S. Cai, K. Zhou, Y. Liang, Q. Chen, and C. Yang, "Compound Control System of Hybrid Distribution Transformer," *IEEE Transactions on Industry Applications*, vol. 56, no. 6, pp. 6360–6373, Nov. 2020.
- [14] Y. Liu, L. Zhang, D. Liang, H. Jin, S. Li, S. Jia, J. Li, H. Liu, Y. Wang, K. Zhou, Y. Gao, S. Cai, D. Li, and S. Feng, "Quasi-Proportional-Resonant Control for the Hybrid Distribution Transformer With LCL-Type Converters," *IEEE Transactions on Industry Applications*, vol. 58, no. 5, pp. 6368–6385, Sep. 2022.
- [15] A. Carreno, M. A. Perez, and M. Malinowski, "State-Feedback Control of a Hybrid Distribution Transformer for Power Quality Improvement of a Distribution Grid," *IEEE Transactions on Industrial Electronics*, vol. 71, no. 2, pp. 1147–1157, Feb. 2024.
- [16] B. Ufnalski, A. Kaszewski, and L. M. Grzesiak, "Particle Swarm Optimization of the Multioscillatory LQR for a Three-Phase Four-Wire Voltage-Source Inverter With an LC Output Filter," *IEEE Transactions on Industrial Electronics*, vol. 62, no. 1, pp. 484–493, Jan. 2015.
- [17] A. Gálceki, M. Michalczuk, B. Ufnalski, and L. M. Grzesiak, "Particle Swarm Optimization of the State Feedback Current Controller with Oscillatory Terms for a Three-Phase Grid-Tie Converter," in *2018 20th European Conference on Power Electronics and Applications (EPE'18 ECCE Europe)*, Sep. 2018, pp. P.1–P.10.
- [18] H. Akagi, A. Nabae, and S. Atoh, "Control Strategy of Active Power Filters Using Multiple Voltage-Source PWM Converters," *IEEE Transactions on Industry Applications*, vol. 1A-22, no. 3, pp. 460–465, May 1986.
- [19] M. Clerc, "The swarm and the queen: Towards a deterministic and adaptive particle swarm optimization," in *Proceedings of the 1999 Congress on Evolutionary Computation-CEC99 (Cat. No. 99TH8406)*, vol. 3, Jul. 1999, pp. 1951–1957 Vol. 3.
- [20] J. Robinson and Y. Rahmat-Samii, "Particle swarm optimization in electromagnetics," *IEEE Transactions on Antennas and Propagation*, vol. 52, no. 2, pp. 397–407, Feb. 2004.